Near itinerancy and slow singlet formation in the triangular lattice $NaRuO_2$

Charles C. Tam,[1] Alon Hendler Avidor,[1] Pritam Bhattacharyya,[2,3] Yongseong Choi,[4] Daniel Haskel,[4] Sven Luther,[5] Hlynur Gretarsson,[6] Liviu Hozoi,[2] and Stephen D. Wilson[1,*]

[1]*Materials Department, University of California Santa Barbara, Santa Barbara, California 93106 USA*

[2]*Institute for Theoretical Solid State Physics, Leibniz IFW Dresden, Helmholtzstraße 20, Dresden 01069, Germany*

[3]*SR University, Warangal, Telangana 506371, India*

[4]*Advanced Photon Source, Argonne National Laboratory, Argonne, Illinois 60439, USA*

[5]*Hochfeld-Magnetlabor Dresden (HLD-EMFL), Helmholtz-Zentrum Dresden-Rossendorf, 01328 Dresden, Germany*

[6]*Deutsches Elektronen-Synchrotron DESY, Hamburg D-22607, Germany*

(Received 6 July 2026; revised 13 October 2026; accepted 21 October 2026; published 10 November 2026)

$NaRuO_2$ forms a delafossitelike structure that contains triangular sublattices of edge-sharing RuO_6 octahedra. It shows no evidence of magnetic order down to 100 mK and persistent spin fluctuations, suggestive of a quantum disordered magnetic ground state. In order to characterize the physical regime from which this disordered state arises, we use resonant inelastic x-ray scattering (RIXS) and x-ray absorption spectroscopy (XAS) at the Ru-$L_{2,3}$ edge, along with pulsed high-field magnetization to characterize both the local electronic structure and the magnetic interactions. We infer significant spin-orbit coupling from XAS measurements. With RIXS, we observe intraorbital excitations, which are damped due to the near itinerancy of the band and suggestive of strong charge fluctuations. Corroborated by fits of the high-field magnetization to a random singlet model, we propose a picture of a nearly itinerant system with strong magnetic and charge fluctuations that destabilize long-range magnetic order.

DOI: 10.1103/stcm-49fx

I. INTRODUCTION

Strong magnetic frustration on triangular lattice compounds has long been known to stabilize unconventional magnetic ground states, ranging from intrinsic quantum disordered states [1–4] to spin supersolid states [5–7] to fascinating non-coplanar spin textures and spin vortex states [8–10]. The character of the electronic wave function decorating the triangular lattice is crucial to determining the ground-state properties, ranging from isotropic spin only moments to spin-orbit-entangled wave functions where strong anisotropies can be engineered.

One of the more fascinating wave functions occurs in the form of $J_{\text{eff}} = 1/2$ spin-orbit-entangled states built from t_{2g}-orbital manifolds. When they are placed in a network of edge-sharing octahedra, strong magnetic frustration results due to the relative amplification of anisotropic, bond-dependent exchange terms. The seminal example of this occurs in spin-orbit-assisted Mott insulators with $J_{\text{eff}} = 1/2$ pseudospins on a nonfrustrated honeycomb lattice. The result is a dominant bond-dependent interaction known as Kitaev exchange, with realizations in materials such as α-$RuCl_3$ [11,12]. In the limit where isotropic Heisenberg exchange vanishes, a spin liquid ground state is predicted [13–15], and there are proposals of unconventional Kitaev-driven states across a host of networks with edge-sharing octahedra [16], including triangular lattices [17].

A competing instability that forms a quantum disordered ground state is the random singlet phase [18–20]. In this scenario, residual disorder suppresses long-range magnetic order, such that the exchange is described by a probability distribution function, which may have a power-law behavior, e.g., $P(J) \sim J^{-\alpha}$. A number of spin liquid candidates have been shown to obey this behavior [21,22], such as the case of $YbMgGaO_4$, where significant Mg-Ga disorder appears to suppress the magnetic order and is shown to form a random singlet state (RSS) rather than a quantum spin liquid (QSL) [23].

An interesting triangular lattice magnet where both strong Kitaev exchange and the potential for disorder effects manifest is the compound $NaRuO_2$, where theoretical models report a large antiferromagnetic Kitaev term [24] and Na-Ru site defects must be carefully managed [25]. $NaRuO_2$ is formed by stacked triangular lattices of NaO_6 and RuO_6 octahedra [Fig. 1(a)], and its magnetic ground state is disordered and characterized by slow, persistent fluctuations [26]. The nature of its electronic ground state and the microscopic origin of these fluctuations remain open questions.

Specifically, in $NaRuO_2$, Ru naively assumes a 3^+ oxidation state with a d^5 configuration, leading to a $J_{\text{eff}} = 1/2$ ground state [24], analogous to α-$RuCl_3$. While the electronic ground state is predicted to be insulating [24,27], consistent with electrical transport data [26], little is known about the character of the Mott phase. In particular, how strong the resulting Mott state is and the potential proximity of strong charge fluctuations remain undetermined experimentally. Equally undetermined is the impact of the dilute defects that persist in polycrystalline samples. Illustrations of possible

*Contact author: stephendwilson@ucsb.edu

 ©2026 American Physical Society

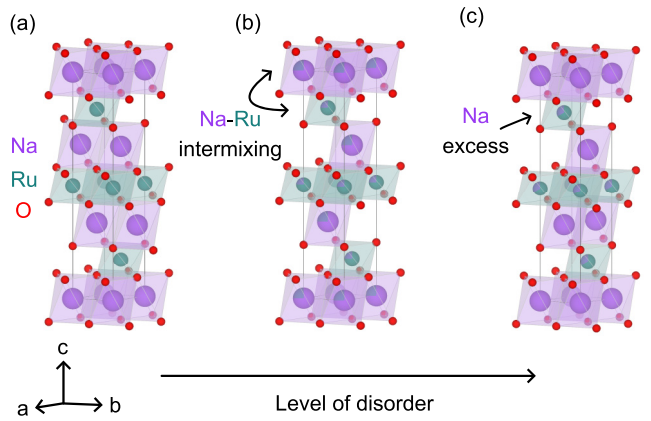


FIG. 1. Possible defect modes in the triangular lattice of $NaRuO_2$. (a) Drawing of the unit cell of pristine $NaRuO_2$. RuO_6 and NaO_6 octahedra have been drawn. (b) Illustration of a Na-Ru site mixing defect in $NaRuO_2$. (c) Illustration of disordered honeycomb Na_2RuO_3, which is equivalent to $NaRuO_2$ with a 1/3 occupation of Na on the Ru site.

defect modes, as discussed in Ref. [25], are seen in Figs. 1(b) and 1(c). Resolving the importance of charge fluctuations and determining the impact of dilute disorder on the magnetic ground state are important questions for resolving the nature of the quantum disordered ground state in $NaRuO_2$.

To clarify these open issues, here we report Ru-$L_{2,3}$-edge resonant inelastic x-ray scattering (RIXS), X-ray absorption spectroscopy (XAS), and pulsed high-field magnetization measurements on polycrystalline $NaRuO_2$ to characterize the nature of its electronic and magnetic ground states. While the SOC strength inferred from XAS is comparable to that of α-$RuCl_3$, a clear $J_{\text{eff}} = 1/2$ excitation is not observed with RIXS, instead overdamped intraorbital excitations appear, reminiscent of a metal. This suggests the dominant role of charge fluctuations in $NaRuO_2$ relative to Kitaev terms in destabilizing magnetic order. We further show that the high-field, low-temperature magnetization can be captured with a random singlet model, where charge fluctuations associated with disorder from dilute Na-Ru intersite mixing [25] suppress the magnetic order.

II. METHODS

Polycrystalline $NaRuO_2$ was synthesized by a solid-state reaction as detailed in Ref. [26]. Polycrystalline samples were densified using spark plasma sintering and were polished to a mirror finish. Samples were measured without cleaving. Ru-L_3-edge RIXS was performed at the IRIXS spectrometer at P01, PETRA-III, DESY, with an energy resolution of around 70 meV [28,29]. RIXS measurements were taken with a fixed incident angle of $\theta = 20^\circ$, a fixed scattering angle of $2\theta = 90^\circ$, and at 20 K. Ru-$L_{2,3}$-edge XAS was performed at APS beamline 4ID, Argonne National Lab, and data were taken in the partial fluorescence yield mode.

XAS data were corrected for self-absorption and normalized such that the L_3-edge absorption jump was unity. Spectra were fit to an arctangent broadened step function to fit the edge jump, and a Lorentzian peak. The center of the step and the Lorentzian were constrained together, and the width of the arctangent was fixed to tabulated values for the Ru-$L_{2,3}$ edges [30] while other parameters were left to float. We fit the RIXS spectra to a multipeak model, corresponding to the multiple inelastic features (phonons, and three higher energy modes A, B, and C). The quasielastic peak was fit with a resolution-limited pseudo-Voigt function, and the phonon with a resolution-limited Gaussian. Mode A was fit to a damped harmonic (DHO) response, while mode B was well-fit with two Gaussians. The tail of mode C was fit with a linear background. The DHO response was given by

$$I(\omega) = A\frac{1}{1-\exp(-\hbar\omega/k_BT)}\frac{\omega_0}{\left(\omega^2-\omega_0^2\right)+\omega^2\gamma^2}, \qquad (1)$$

where ω_0 is the DHO pole frequency and γ is the damping factor. With this definition, the DHO is damped when $\omega_0 > \gamma/2$ and overdamped when $\omega_0 < \gamma/2$.

Pulsed high-field magnetization measurements were conducted at the Dresden High Magnetic Field Laboratory, HLD-HZDR, using a magnetometer with a compensated pickup-coil system and a home-built ^{3}He cryostat. Polycrystalline $NaRuO_2$ was packed in a quartz capillary in an Ar glovebox and flame-sealed. High-field measurements were calibrated to isothermal $M(H)$ curves taken with a Quantum Design MPMS. Magnetic susceptibility and magnetization measurements were performed in a Quantum Design MPMS, on $NaRuO_2$ powder loaded in a brass holder.

Magnetic measurements were fit to an RSS model, which is detailed in Ref. [21]. In this model, the magnetization is given by

$$M_{\text{RSS}}(H) = \int_0^\infty \mathrm{d}J P(J)\frac{2\mu\sinh(\beta\mu H)}{2\cosh(\beta\mu H)+1+e^{\beta J}}, \qquad (2)$$

where $\beta = 1/k_BT$, H is the magnetic field, and $P(J) = \theta(J_0 - J)J^{-\alpha}$ is an empirical form of the exchange probability distribution function, where θ is a normalizing constant. Here, α is the power-law exponent and J_0 is a cutoff scale to avoid a diverging integral. We fix J_0 to 100 K for all fits. From Eq. (2), it follows the magnetic susceptibility is given by $\chi_{\text{RS}} = \partial M_{\text{RS}}/\partial H$. We fit with a Van Vleck term, i.e., $\chi(T) = \chi_{\text{RS}}(T) + \chi_0$, and $M(H) = M_{\text{RS}}(H) + \chi_0 H$. Since fits are highly background dependent, the value of χ_0 is constrained to be the same for all fits.

Multiplet-structure quantum chemical calculations were performed with the focus on the branching ratio (BR), using the MOLPRO [31] package. Finite clusters and embeddings as described in Refs. [32,33] were employed to compute and compare BRs in $4d^5$ $NaRuO_2$ and $4d^5$ $RuCl_3$. The BRs were obtained following the procedure outlined in Ref. [34], on the basis of complete-active-space self-consistent-field computations [35,36] for an average of the $^2T_{2g}\, t_{2g}^5$, $^4T_{1g}$ and $^4T_{2g}\, t_{2g}^4 e_g^1$, $^6A_{1g}\, t_{2g}^3 e_g^2$, and low-lying $^2A_{2g}$, $^2T_{1g}$, $^2T_{2g}$, and $^2E_g\, t_{2g}^4 e_g^1$ states. In the subsequent spin-orbit treatment [37], all possible $4d^5$ states were included.

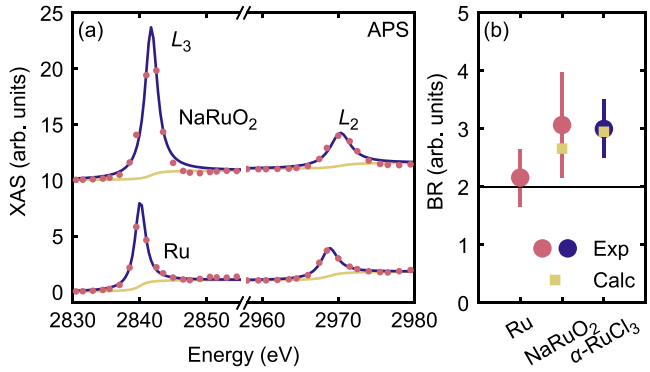


FIG. 2. Branching ratios determined from Ru-L XAS. (a) XAS taken across the Ru L_3 and L_2 edges, on Ru and $NaRuO_2$. Data are fit to an arctangent step function and Lorentzian, defined in the methods. (b) Experimental branching ratio (BR), defined as the fit intensity at L_3 divided by the intensity at L_2 for Ru, $NaRuO_2$, and α-$RuCl_3$. The experimental BR for α-$RuCl_3$ is taken from Ref. [11]. Details on the BR calculation for $NaRuO_2$ and α-$RuCl_3$ are given in the methods. Energy resolution in the presented dataset was insufficient to identify finer detail in the $L_{3,2}$ peaks.

III. RESULTS

A. Electronic structure

As an initial probe for the role of SOC in the ground-state wave function of Ru^{3+}, XAS measurements were performed across the Ru-$L_{2,3}$ edges. Here the Ru-L_2 edge corresponds to exciting $2p_{1/2} \rightarrow 4d$ while the L_3 edge is $2p_{3/2} \rightarrow 4d$. The angular part of the spin-orbit interaction $L \cdot S$ is related to the relative intensities of the L_3- and L_2-edge absorption peaks [38–41] and is a conventional metric for classifying the strength of SOC in spin-orbit-entangled wave functions [42,43]. To investigate how the SOC in $NaRuO_2$ compares to other strongly spin-orbit-entangled systems, XAS data for $NaRuO_2$ is plotted in Fig. 2 and compared to Ru metal, as well as α-$RuCl_3$ [11]. We note that generally, the BR for ruthenates is less than that of iridates. Taking the cases of Sr_2IrO_4 and α-$RuCl_3$, both have electron configuration d^5. The $5d$ states in the iridate are expected to have more SOC than those in the ruthenate, since the SOC scales with Z^2 (account for screening). Accordingly, the measured SOC in Sr_2IrO_4 is around 0.4 eV [44], while in α-$RuCl_3$ it is 0.15 eV [45]. Since the BR is impacted by the degree that SOC mixes t_{2g} and e_g states, it follows the BR for ruthenates with smaller SOC and larger U is less than that for iridates.

XAS data at the L_3 and L_2 edges were modeled as discussed in the methods section to determine their BRs (i.e., I_{L_3}/I_{L_2}). Fits are overplotted with the XAS spectra in Fig. 2(a), and the extracted branching ratios for the two measured materials are plotted in Fig. 2(b), alongside the BR for α-$RuCl_3$ [11]. The BR for Ru metal is around 2, which is the expected statistical BR for a metal with a quenched spin-orbit interaction. In contrast, the BR value for $NaRuO_2$ is close to 3, similar to that found for the $J_{\text{eff}} = 1/2$ state in α-$RuCl_3$ [11]. We also note $NaRuO_2$ has a similar BR to other $4d$ oxides with similar electron counts, namely, d^4 $SrRuO_3/SrTiO_3$ films [46] and d^5 Li_2RhO_3 [47]. This is consistent with the picture of a $J_{\text{eff}} = 1/2$ Mott state as the parent electronic phase for $NaRuO_2$.

Quantum chemical computations yield a BR of 2.65 for $NaRuO_2$, somewhat lower than that extracted from experiment, but still in the region corresponding to $J_{\text{eff}} \approx 1/2$ moments. Slight underestimation of the BR was also found in quantum chemical calculations on, e.g., Ba_2IrO_4 [34]. For comparison, a BR of 2.9 was obtained computationally for $RuCl_3$; experimentally, values of 3 [11] and 3.6 [48] were reported for the latter compound. The smaller BR for $NaRuO_2$ in the embedded-cluster quantum chemical computations can be understood on the basis of two effects : (i) a larger trigonal splitting ($\approx$0.11 eV in $NaRuO_2$ [32] vs $\approx$0.07 eV in $RuCl_3$ [33]), which yields a BR lower than the 2.75 value corresponding to pristine, cubic-environment $J_{\text{eff}} = 1/2$ moments with negligible configuration-interaction effects and second-order SOCs within the $4d^5$ manifold; (ii) a larger octahedral t_{2g}-e_g splitting, with $t_{2g} \rightarrow e_g$ excitations starting at $\approx$1.6 eV in $NaRuO_2$ (see Ref. [32] and next paragraphs) and at $\approx$1.3 eV in $RuCl_3$ [33,48], which makes configuration-interaction effects and second-order SOCs somewhat less effective in $NaRuO_2$.

To explore the Mott state further, the low-energy Ru electronic states were studied by RIXS measurements at the Ru-L_3 edge. An overview of the RIXS data can be seen in Fig. 3. To start, XAS data taken across the L_3 edge are plotted in Fig. 3(a), where two peaks appear at 2838 and 2840.5 eV. Since $NaRuO_2$ possesses a d^5 filling, this corresponds to exciting into t_{2g} and e_g states. The energy separation of the two peaks is around 2.5 eV, which is consistent with the expected crystal field splitting. This is a similar value to similarly coordinated $SrRuO_3$ [49].

A RIXS intensity map as a function of incident photon energy and photon energy loss is plotted in Fig. 3(b). Three main features resonate across the L_3 edge, which we label as features A, B, and C. In addition to these features, close to zero energy, a quasielastic peak and phonon mode appear. The RIXS spectra were fit to a model, defined in the methods section, that parametrizes the high-energy electronic modes A, B, and C. Sample RIXS spectra collected at fixed incident energy, overplotted with their fit components, are presented in Fig. 4(b).

Starting from high energy and working downward, feature C has the energy scale of a charge-transfer mode. Mode B is centered near 3-eV energy loss, suggestive of an interorbital excitation between $4d$ t_{2g} and e_g states. This corresponds well to interorbital excitations reported in other ruthenates (see, e.g., Refs. [50–52]). Finally, mode A appears near 500 meV. Since this resonates at the t_{2g} prepeak, this mode potentially arises from intraorbital excitations within the t_{2g} manifold, or, as discussed later, it represents a highly damped spin-orbit exciton. Modes A, B, and C are all present across the Ru-L_3 edge, and all show moderate enhancement at resonance.

For most of the incident energy range, the fit DHO center and damping rate for mode A remain constant, with average values of $\omega_0 \approx 1000$ meV and $\gamma \approx 1700$ meV, meaning the mode is damped due to our definition of the DHO response in Eq. (1). Near the t_{2g} resonance, mode A starts moving to higher energy and becomes overdamped at 2839 eV. This is more apparent when the spectra are normalized to mode A,

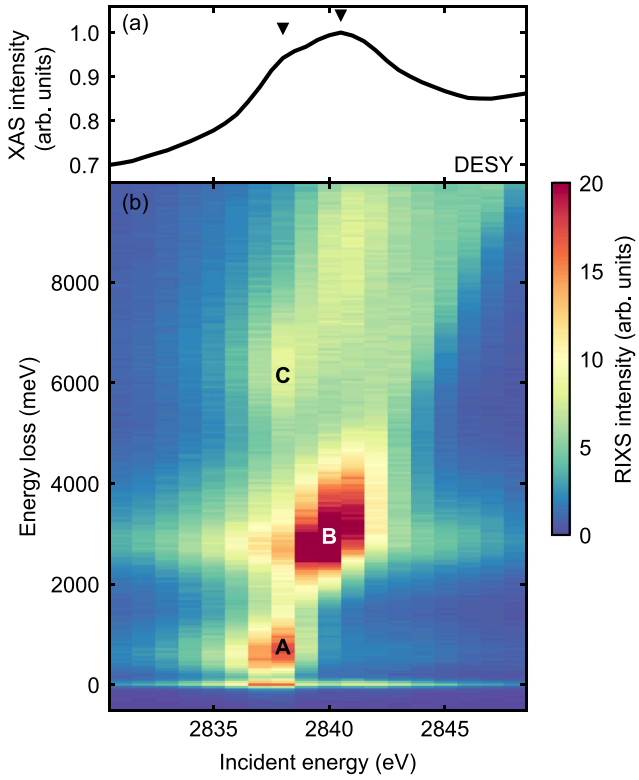


FIG. 3. Ru-L_3-edge resonant inelastic X-ray scattering on polycrystalline $NaRuO_2$. (a) XAS over the Ru-L_3 edge, taken in fluorescence yield at room temperature. Marked peaks correspond to excitations into t_{2g} and e_g states. Normalization and self-absorption corrections have not been applied due to the small energy range collected. (b) RIXS energy map over the L_3 edge, showing three main features labeled A, B, and C. RIXS data were momentum-averaged, as the sample is polycrystalline, and taken at 20 K.

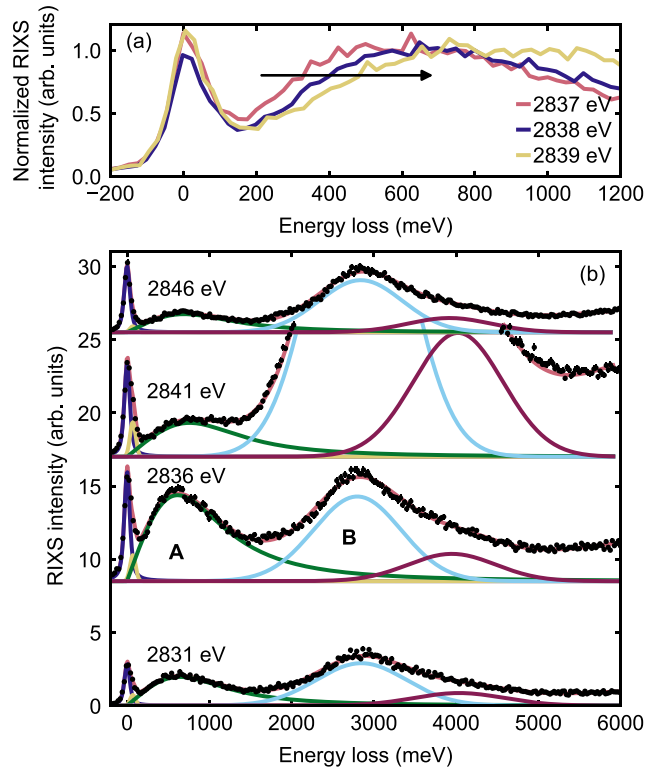


FIG. 4. Energy-dependent Ru-L_3-edge RIXS spectra. (a) RIXS spectra normalized to intensity at 500 meV, across the L_3 edge. (b) RIXS spectra at various incident energies, showing their fits.

as plotted in Fig. 4(a). The mode is dispersing too slowly to be consistent with fluorescence, and instead the damped mode is reminiscent of a metal, where the local t_{2g} transitions hybridize with the itinerant electrons to give a damped, slowly dispersing mode.

Similar damped intraorbital excitations have been observed in RIXS studies of other metallic ruthenates [51,53,54] and are not present in insulating ruthenates with a clearly defined gap [51,52,55]. There is no clearly defined excitation that can be assigned to $J_{\text{eff}} = 1/2$ or to $J_{\text{eff}} = 3/2$, as seen in insulating compounds with a $J_{\text{eff}} = 1/2$ ground state [45,56]. However, we cannot rule out it is absent as it may be damped by the highly itinerant intraorbital fluctuations. This suggests that the Mott state in $NaRuO_2$ is weakened by the itinerancy of the system.

We also note the resonance effect of the quasielastic line. To see it more clearly, we plot the fitted intensity of the pseudovoigt used to model quasielastic scattering as a function of incident energy in Fig. 5(a). We see a pronounced resonance effect peaked at $E_i \approx 2837$ eV, which is the t_{2g} resonance. Given the relatively poor energy resolution of $\Delta E \approx 70$ meV, this would integrate many low-energy features into the quasielastic scattering channel, e.g., phonons and spin fluctuations. Phonons in $4d$ systems tend to have a weaker resonance effect and also tend to resonate at the higher-energy e_g resonance (cf. Refs. [45,50,55]). We can also preclude any static order in the charge channel, e.g., charge density wave fluctuations, since the sample is polycrystalline. Therefore, it is likely these are low-energy spin fluctuations that are being integrated into the quasielastic channel that are giving rise to the strong resonance effect. To compare with results from inelastic neutron scattering (INS) measurements, we plot a RIXS spectrum at $E_i = 2837$ eV along with a momentum integrated energy cut from Ref. [26], in Fig. 5(b). A peak in the

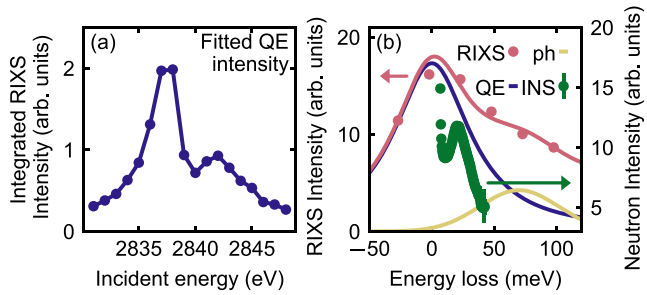


FIG. 5. Low-energy excitations in $NaRuO_2$. (a) Fitted quasielastic RIXS intensity, as a function of incident energy. (b) RIXS response, taken at 2837 eV, where the data points are in red, fit is a red line, and quasielastic and phonon fit components are in blue and yellow. In green is the Q-integrated energy cut inelastic neutron scattering data, taken at 1.8 K. The integration window is [0, 2] Å^{-1}. Neutron data are from Ref. [26].

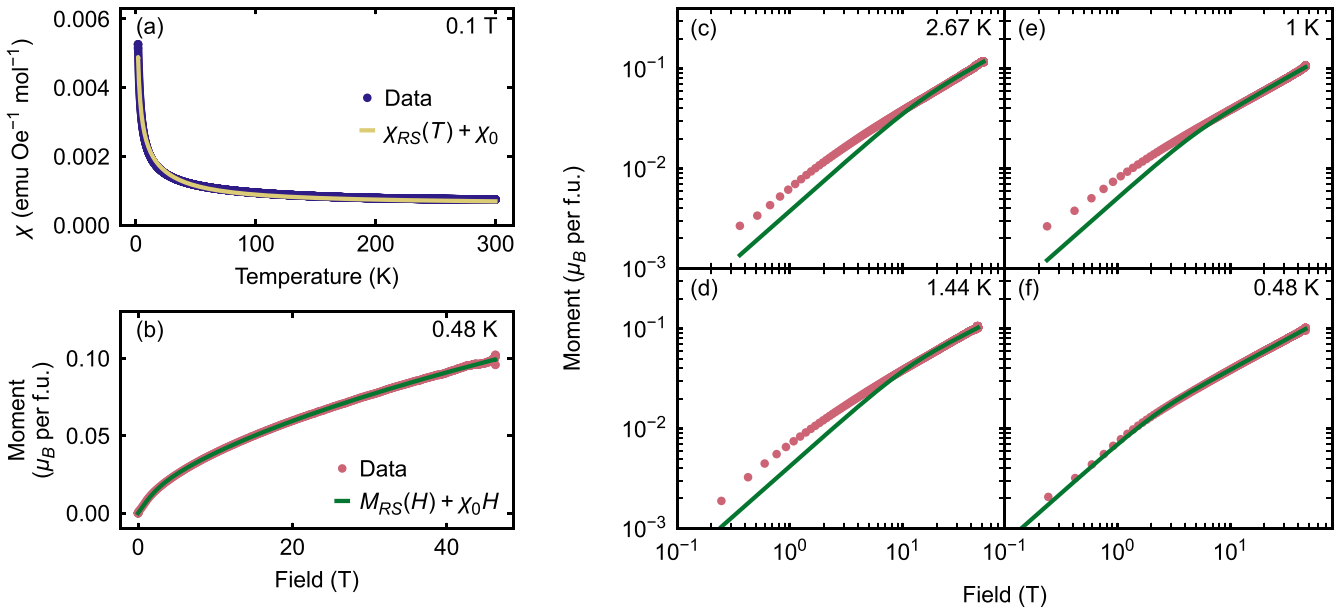


FIG. 6. Random singlet fits to magnetic measurements of $NaRuO_2$. Fits of the random singlet model to (a) magnetization taken at $T = 0.48$ K up to 45 T and (b) magnetic susceptibility at $H = 0.1$ T. Definitions of $M_{\rm RS}(H)$ and $\chi_{\rm RS}(T)$ are given in the main text. (c)–(f) RSS fits to high-field magnetization at various temperatures on a log-log scale.

INS response at around 30 meV is consistent with being spin fluctuations [26], which is in turn consistent with the energy scales of the quasielastic RIXS peak. This corroborates the presence of low-energy spin fluctuations, which are present when measured with RIXS at 20 K and are also present down to 1.8 K [26].

B. Magnetic ground state

Turning now to the origin of the low-energy magnetic excitations in $NaRuO_2$, magnetization data were collected at low temperatures and under high magnetic fields. The temperature dependence of magnetic susceptibility, taken under an applied field of $\mu_0 H = 0.1$ T is plotted in Fig. 6(a). Consistent with earlier results, there is no evidence of magnetic ordering down to the lowest temperature measured of 1.8 K. Models of such a response, however, can be ambiguous. Fits with a large Van Vleck-like constant susceptibility dressed with either a dilute concentration of paramagnetic impurities (parametrized as ≈2% spin-1/2 moments from Ref. [26]) or as a slow freezing of moments perform equally well. We note the inverse susceptibility does not fit a Curie-Weiss form, so obtaining an effective moment is not possible.

To gain deeper insight into the origin of the enhanced low-temperature susceptibility, isothermal high-field measurements were performed. Pulsed high-field magnetization data taken at $T = 0.48$ K are plotted in Fig. 6(b). Above $\approx$ 20 T, the slope of magnetization saturates, signifying a constant susceptibility. The total moment approaches around 0.1 μ_B per Ru ion at 45 T, consistent with the large magnetic exchange expected for this system. The lowest temperature 0.48 K isothermal data were fit to a random singlet RSS model Eq. (2) [Fig. 6(f)]. This describes the data well, but quickly breaks down at 1 K and higher temperatures [Figs. 6(c)–6(e)], which will be discussed more later. From the fits, the power-law exponent α can be extracted, which is summarized in Table I and compared with the same RSS model fit to the temperature dependent susceptibility data in Fig. 6(a). The susceptibility of the RSS model was taken as the derivative of the magnetization Eq. (2) and the relatively large Van Vleck term of $\chi_0 = 5.9(2) \times 10^{-4}$ emu Oe mol^{-1} was kept fixed across all fits. The α values between fits yield good agreement between the $\chi(T)$ and $M(H)$ fits, with $\alpha \approx 0.4$ to 0.5. This suggests that the power-law scaling of the RSS exchange probability holds at the lowest temperature measured.

IV. DISCUSSION AND CONCLUSIONS

Empirically, RIXS measurements suggest that $NaRuO_2$ is more itinerant than transport measurements suggest. As a result, the presence of a $J_{\rm eff} = 1/2$ to $J_{\rm eff} = 3/2$ exciton mode is not clear due to the strong damping from charge fluctuations. The SOC strength inferred from XAS is nevertheless comparable to α-$RuCl_3$ and consistent with a $J_{\rm eff} = 1/2$ state; however, we note that our XAS measurements lack the resolution to resolve the structure of the L_2 peak. We are therefore unable to comment on the nature of the $2p_{1/2} \rightarrow t_{2g}$ transition, which should be forbidden for a pure $J_{\rm eff} = 1/2$ ground state [11].

TABLE I. RSS fit results. Fit values for the power-law exponent α to the various datasets. The RSS model is defined in Sec. II.

Measurement	α
$\chi(T)$	0.491(2)
$M(H, T = 0.48\ \text{K})$	0.434(1)
$M(H, T = 1\ \text{K})$	0.393(2)

A good comparator of a Mott state in the metallic limit is $Ru(Br_{1-x}I_x)_3$. While $RuBr_3$ is a spin-orbit-entangled Mott insulator [57], RuI_3 is a semimetal [58,59], and a metal-insulator transition (MIT) occurs in intermediate compositions [60]. RIXS on these materials reveals a $J_{\text{eff}} = 1/2$ excitation that is present in both $RuBr_3$ and RuI_3, although it is more damped in RuI_3 [51]. This is notable as this demonstrates the $J_{\text{eff}} = 1/2$ state can exist in a metal, although this case is distinct from $NaRuO_2$, as it is thought the bandwidth of the larger halogen p orbitals drives the MIT [51], rather than the intrinsic weak Mott state in $NaRuO_2$ which we infer from our measurements.

Transport data reported earlier show a clear insulating/semiconducting behavior in ≈95% density samples [26], precluding trivial grain boundary effects from dominating the response. Instead of a clean gap, variable-range hopping models better describe transport data, which are consistent with a polluted Mott gap and the low-energy electronic excitations resolved in RIXS. Together, this suggests that the Mott state in $NaRuO_2$ is only marginally stable and that substantial charge fluctuations must be accounted for.

Successful fits of magnetization data to an RSS model at the lowest measured temperature suggest that the Ru moments transition into a random singlet phase below ≈1 K. This seemingly resolves an earlier puzzle of a small entropy anomaly and partial freezing previously observed near 1.5 K in heat capacity and susceptibility data [26]. While the small entropy change and weak cusp observed in susceptibility were consistent with a few percent fraction of free, impurity moments freezing, muon spin relaxation (μSR) measurements resolved the *global* appearance of an inhomogeneous field distribution near this same temperature. This suggests that the moments globally cross over into a new low-temperature phase below the 1.5-K energy scale, which is effectively probed by our high-field magnetization measurements at 0.5 K. The agreement with the RSS model suggests that the onset of inhomogeneous spin fluctuations detected in μSR is the onset of slow singlet formation across the network of Ru moments. This is potentially driven by the residual (several percent) chemical disorder likely present in the lattice, though we note that μSR also detects persistent, slow spin fluctuations in this low-temperature state.

The synthesis of polycrystalline $NaRuO_2$ involves an excess of Ru which seems to mitigate the amount of Na-Ru site disorder. Fitting free spin impurity fractions from prior susceptibility and heat capacity data yields ≈2% molar fractions per formula unit, alongside a lower bound confidence for site mixing from neutron diffraction of around 5% [26]. This fraction is substantially smaller than canonical RSS materials; however, it can still dominate the magnetization signal relative to a quantum paramagnetic background. Alternatively, in global models of a random singlet phase, J_2/J_1-Δ models of disorder on an $S = 1/2$ triangular lattice predict a disordered spin phase, consistent with an RSS phase, as a fan above the QSL phase, for finite $\Delta > 0$ [20]. In this picture of a global RSS phase, if $NaRuO_2$ is indeed proximate to a QSL in its pristine state, a small 2–5% site mixing could be enough to destabilize the QSL into an RSS phase.

Above 1.5 K, fits to an RSS model break down, consistent with μSR's observation of dynamic moments in this regime [26] and supportive of the notion of a crossover below this temperature. Heat capacity data fit to different power laws above and below this crossover, which preclude fits of C_p (T) to an RSS model. Higher field specific heat measurements ($\mu_0 H > 14$ T) are of interest for more fully shifting the crossover anomaly upward in temperature and obtaining a larger dynamic range for testing RSS fits.

Together our results paint a refined picture of the electronic state that gives rise to the unusual quantum disordered phase reported in $NaRuO_2$. Rather than a strongly local model involving strong Kitaev and anisotropic extended exchange terms with a fully gapped charge degree of freedom, RIXS and XAS data instead emphasize a starting point of a weak Mott phase with strong charge fluctuations. While the starting $J_{\text{eff}} = 1/2$ wave functions are similar, $NaRuO_2$ is therefore distinct from α-$RuCl_3$, likely due to its enhanced bandwidth. Instead, the strong role of charge fluctuations and the propensity of Ru to form dimers invites a closer comparison to organic Mott systems [61]. This weak Mott state paired with small levels of chemical disorder freezes into a state consistent with RSS models, though there is a clear crossover above 1.5 K into a dynamic spin state. Whether or not this crossover is intrinsic or disorder-driven will require investigation of higher-purity specimens, such as single-crystal samples.

ACKNOWLEDGMENTS

We acknowledge helpful discussions with Pavel Volkov. This work was supported by the U.S. Department of Energy, Office of Science, Basic Energy Sciences, under Award No. DE-SC0017752. Research was performed using facilities at the Advanced Photon Source, a U.S. Department of Energy (DOE), Office of Science user facility operated for the DOE Office of Science by the Argonne National Laboratory under Contract No. DE-AC02-06CH11357. We also acknowledge DESY—a member of the Helmholtz Association HGF—for access to beam time. We also acknowledge support of the HLD at HZDR, member of the European Magnetic Field Laboratory (EMFL).

DATA AVAILABILITY

The data that support the findings of this article are openly available [62].

[1] P. Anderson, Resonating valence bonds: A new kind of insulator? Mater. Res. Bull. **8**, 153 (1973).

[2] Y. Shimizu, K. Miyagawa, K. Kanoda, M. Maesato, and G. Saito, Spin liquid state in an organic Mott insulator with a triangular lattice, Phys. Rev. Lett. **91**, 107001 (2003).

[3] S. Nakatsuji, Y. Nambu, H. Tonomura, O. Sakai, S. Jonas, C. Broholm, H. Tsunetsugu, Y. Qiu, and Y. Maeno, Spin disorder on a triangular lattice, Science **309**, 1697 (2005).

[4] S. Yamashita, Y. Nakazawa, M. Oguni, Y. Oshima, H. Nojiri, Y. Shimizu, K. Miyagawa, and K. Kanoda, Thermodynamic

properties of a spin-1/2 spin-liquid state in a κ-type organic salt, Nat. Phys. **4**, 459 (2008).

[5] T. Momoi and K. Totsuka, Magnetization plateaus of the Shastry-Sutherland model for $SrCu_2(BO_3)_2$: Spin-density wave, supersolid, and bound states, Phys. Rev. B **62**, 15067 (2000).

[6] P. Sengupta and C. D. Batista, Field-induced supersolid phase in spin-one Heisenberg models, Phys. Rev. Lett. **98**, 227201 (2007).

[7] D. Yamamoto, G. Marmorini, and I. Danshita, Quantum phase diagram of the triangular-lattice XXZ model in a magnetic field, Phys. Rev. Lett. **112**, 127203 (2014).

[8] T. Okubo, S. Chung, and H. Kawamura, Multiple-q states and the skyrmion lattice of the triangular-lattice Heisenberg antiferromagnet under magnetic fields, Phys. Rev. Lett. **108**, 017206 (2012).

[9] T. Kurumaji, T. Nakajima, M. Hirschberger, A. Kikkawa, Y. Yamasaki, H. Sagayama, H. Nakao, Y. Taguchi, T.-h. Arima, and Y. Tokura, Skyrmion lattice with a giant topological Hall effect in a frustrated triangular-lattice magnet, Science **365**, 914 (2019).

[10] P. Park, W. Cho, C. Kim, Y. An, Y.-G. Kang, M. Avdeev, R. Sibille, K. Iida, R. Kajimoto, K. H. Lee, W. Ju, E.-J. Cho, H.-J. Noh, M. J. Han, S.-S. Zhang, C. D. Batista, and J.-G. Park, Tetrahedral triple-Q magnetic ordering and large spontaneous Hall conductivity in the metallic triangular antiferromagnet $Co_{1/3}TaS_2$, Nat. Commun. **14**, 8346 (2023).

[11] K. W. Plumb, J. P. Clancy, L. J. Sandilands, V. V. Shankar, Y. F. Hu, K. S. Burch, H.-Y. Kee, and Y.-J. Kim, α-$RuCl_3$: A spin-orbit assisted Mott insulator on a honeycomb lattice, Phys. Rev. B **90**, 041112(R) (2014).

[12] J. A. Sears, M. Songvilay, K. W. Plumb, J. P. Clancy, Y. Qiu, Y. Zhao, D. Parshall, and Y.-J. Kim, Magnetic order in α-$RuCl_3$: A honeycomb-lattice quantum magnet with strong spin-orbit coupling, Phys. Rev. B **91**, 144420 (2015).

[13] A. Kitaev, Anyons in an exactly solved model and beyond, Ann. Phys. **321**, 2 (2006).

[14] G. Jackeli and G. Khaliullin, Mott insulators in the strong spin-orbit coupling limit: From Heisenberg to a quantum compass and Kitaev models, Phys. Rev. Lett. **102**, 017205 (2009).

[15] J. Chaloupka, G. Jackeli, and G. Khaliullin, Kitaev-Heisenberg model on a honeycomb lattice: Possible exotic phases in iridium oxides A_2IrO_3, Phys. Rev. Lett. **105**, 027204 (2010).

[16] I. Kimchi and A. Vishwanath, Kitaev-Heisenberg models for iridates on the triangular, hyperkagome, kagome, fcc, and pyrochlore lattices, Phys. Rev. B **89**, 014414 (2014).

[17] K. Li, S.-L. Yu, and J.-X. Li, Global phase diagram, possible chiral spin liquid, and topological superconductivity in the triangular Kitaev-Heisenberg model, New J. Phys. **17**, 043032 (2015).

[18] T. Shimokawa, K. Watanabe, and H. Kawamura, Static and dynamical spin correlations of the $s = 1/2$ random-bond antiferromagnetic Heisenberg model on the triangular and kagome lattices, Phys. Rev. B **92**, 134407 (2015).

[19] I. Kimchi, J. P. Sheckelton, T. M. McQueen, and P. A. Lee, Scaling and data collapse from local moments in frustrated disordered quantum spin systems, Nat. Commun. **9**, 4367 (2018).

[20] H.-Q. Wu, S.-S. Gong, and D. N. Sheng, Randomness-induced spin-liquid-like phase in the spin-1/2 J_1-J_2 triangular Heisenberg model, Phys. Rev. B **99**, 085141 (2019).

[21] P. A. Volkov, C.-J. Won, D. I. Gorbunov, J. Kim, M. Ye, H.-S. Kim, J. H. Pixley, S.-W. Cheong, and G. Blumberg, Random singlet state in $Ba_5CuIr_3O_{12}$ single crystals, Phys. Rev. B **101**, 020406(R) (2020).

[22] J. Khatua, M. Gomilšek, J. C. Orain, A. M. Strydom, Z. Jagličić, C. V. Colin, S. Petit, A. Ozarowski, L. Mangin-Thro, K. Sethupathi, M. S. Ramachandra Rao, A. Zorko, and P. Khuntia, Signature of a randomness-driven spin-liquid state in a frustrated magnet, Commun. Phys. **5**, 99 (2022).

[23] I. Kimchi, A. Nahum, and T. Senthil, Valence bonds in random quantum magnets: Theory and application to $YbMgGaO_4$, Phys. Rev. X **8**, 031028 (2018).

[24] A. Razpopov, D. A. S. Kaib, S. Backes, L. Balents, S. D. Wilson, F. Ferrari, K. Riedl, and R. Valentí, A $J_{\text{eff}} = 1/2$ Kitaev material on the trianglur lattice: The case of $NaRuO_2$, npj Quantum Mater. **8**, 36 (2023).

[25] B. R. Ortiz, P. M. Sarte, A. H. Avidor, and S. D. Wilson, Defect control in the Heisenberg-Kitaev candidate material $NaRuO_2$, Phys. Rev. Mater. **6**, 104413 (2022).

[26] B. R. Ortiz, P. M. Sarte, A. H. Avidor, A. Hay, E. Kenney, A. I. Kolesnikov, D. M. Pajerowski, A. A. Aczel, K. M. Taddei, C. M. Brown, C. Wang, M. J. Graf, R. Seshadri, L. Balents, and S. D. Wilson, Quantum disordered ground state in the triangular-lattice magnet $NaRuO_2$, Nat. Phys. **19**, 943 (2023).

[27] A. Bouhmouche, I. Rhrissi, A. Jabar, and R. Moubah, Electronic, optical, and thermodynamic properties of a quantum spin liquid candidate $NaRuO_2$ *ab-initio* investigation, Mater. Chem. Phys. **314**, 128860 (2024).

[28] H. Gretarsson, D. Ketenoglu, M. Harder, S. Mayer, F.-U. Dill, M. Spiwek, H. Schulte-Schrepping, M. Tischer, H.-C. Wille, B. Keimer, and H. Yavaş, IRIXS: A resonant inelastic x-ray scattering instrument dedicated to x-rays in the intermediate energy range, J. Synchrotron Radiat. **27**, 538 (2020).

[29] M. Sundermann, M. Harder, A. H. Said, B. Keimer, and H. Gretarsson, Dispersion-compensated Rowland spectrometer: Implications for uranium VB-RIXS, J. Synchrotron Radiat. **33**, 218 (2026).

[30] M. O. Krause and J. H. Oliver, Natural widths of atomic K and L levels, $K\alpha$ X-ray lines and several KLL Auger lines, J. Phys. Chem. Ref. Data **8**, 329 (1979).

[31] H.-J. Werner, P. J. Knowles, G. Knizia, F. R. Manby, and M. Schütz, Molpro: A general-purpose quantum chemistry program package, WIREs Comput. Mol. Sci. **2**, 242 (2012).

[32] P. Bhattacharyya, N. A. Bogdanov, S. Nishimoto, S. D. Wilson, and L. Hozoi, $NaRuO_2$: Kitaev-Heisenberg exchange in triangular-lattice setting, npj Quantum Mater. **8**, 52 (2023).

[33] R. Yadav, N. A. Bogdanov, V. M. Katukuri, S. Nishimoto, J. van den Brink, and L. Hozoi, Kitaev exchange and field-induced quantum spin-liquid states in honeycomb α-$RuCl_3$, Sci. Rep. **6**, 37925 (2016).

[34] V. M. Katukuri, K. Roszeitis, V. Yushankhai, A. Mitrushchenkov, H. Stoll, M. van Veenendaal, P. Fulde, J. van den Brink, and L. Hozoi, Electronic structure of low-dimensional $4d^5$ oxides: Interplay of ligand distortions, overall lattice anisotropy, and spin-orbit interactions, Inorg. Chem. **53**, 4833 (2014).

[35] T. Helgaker, P. Jørgensen, and J. Olsen, *Molecular Electronic Structure Theory* (Wiley & Sons, Chichester, England, 2000).

[36] D. A. Kreplin, P. J. Knowles, and H.-J. Werner, MCSCF optimization revisited. II. Combined first- and second-order orbital

optimization for large molecules, J. Chem. Phys. **152**, 074102 (2020).
[37] A. Berning, M. Schweizer, H.-J. Werner, P. J. Knowles, and P. Palmieri, Spin-orbit matrix elements for internally contracted multireference configuration interaction wavefunctions, Mol. Phys. **98**, 1823 (2000).
[38] G. van der Laan and B. T. Thole, Local probe for spin-orbit interaction, Phys. Rev. Lett. **60**, 1977 (1988).
[39] B. T. Thole and G. van der Laan, Branching ratio in x-ray absorption spectroscopy, Phys. Rev. B **38**, 3158 (1988).
[40] B. T. Thole and G. van der Laan, Linear relation between x-ray absorption branching ratio and valence-band spin-orbit expectation value, Phys. Rev. A **38**, 1943 (1988).
[41] G. van der Laan, K. T. Moore, J. G. Tobin, B. W. Chung, M. A. Wall, and A. J. Schwartz, Applicability of the spin-orbit sum rule for the actinide $5f$ states, Phys. Rev. Lett. **93**, 097401 (2004).
[42] M. A. Laguna-Marco, D. Haskel, N. Souza-Neto, J. C. Lang, V. V. Krishnamurthy, S. Chikara, G. Cao, and M. van Veenendaal, Orbital magnetism and spin-orbit effects in the electronic structure of $BaIrO_3$, Phys. Rev. Lett. **105**, 216407 (2010).
[43] J. P. Clancy, N. Chen, C. Y. Kim, W. F. Chen, K. W. Plumb, B. C. Jeon, T. W. Noh, and Y.-J. Kim, Spin-orbit coupling in iridium-based $5d$ compounds probed by x-ray absorption spectroscopy, Phys. Rev. B **86**, 195131 (2012).
[44] B. Zwartsenberg, R. P. Day, E. Razzoli, M. Michiardi, N. Xu, M. Shi, J. D. Denlinger, G. Cao, S. Calder, K. Ueda, J. Bertinshaw, H. Takagi, B. J. Kim, I. S. Elfimov, and A. Damascelli, Spin-orbit-controlled metal–insulator transition in Sr_2IrO_4, Nat. Phys. **16**, 290 (2020).
[45] H. Suzuki, H. Liu, J. Bertinshaw, K. Ueda, H. Kim, S. Laha, D. Weber, Z. Yang, L. Wang, H. Takahashi, K. Fürsich, M. Minola, B. V. Lotsch, B. J. Kim, H. Yavaş, M. Daghofer, J. Chaloupka, G. Khaliullin, H. Gretarsson, and B. Keimer, Proximate ferromagnetic state in the Kitaev model material α-$RuCl_3$, Nat. Commun. **12**, 4512 (2021).
[46] U. Lamichhane, B. Sankhi, N. Kundu, G. Fabbris, Y. Choi, D. Haskel, J. L. McChesney, Y. Cao, J. Li, V. Bisogni, M. F. Borunda, and D. Meyers, Electronic reconstruction in confined $SrRuO_3$ monolayers, Phys. Rev. B **110**, 235104 (2024).
[47] F. Bahrami, X. Hu, Y. Du, O. I. Lebedev, C. Wang, H. Luetkens, G. Fabbris, M. J. Graf, D. Haskel, Y. Ran, and F. Tafti, First demonstration of tuning between the Kitaev and Ising limits in a honeycomb lattice, Sci. Adv. **8**, eabl5671 (2022).
[48] B. W. Lebert, S. Kim, V. Bisogni, I. Jarrige, A. M. Barbour, and Y.-J. Kim, Resonant inelastic x-ray scattering study of α-$RuCl_3$: A progress report, J. Phys.: Condens. Matter **32**, 144001 (2020).
[49] J. Zhang, L. Cheng, H. Cao, M. Bao, J. Zhao, X. Liu, A. Zhao, Y. Choi, H. Zhou, P. Shafer, and X. Zhai, The exceedingly strong two-dimensional ferromagnetism in bi-atomic layer $SrRuO_3$ with a critical conduction transition, Nano Res. **15**, 7584 (2022).
[50] H. Takahashi, H. Suzuki, J. Bertinshaw, S. Bette, C. Mühle, J. Nuss, R. Dinnebier, A. Yaresko, G. Khaliullin, H. Gretarsson, T. Takayama, H. Takagi, and B. Keimer, Nonmagnetic $J = 0$ state and spin-orbit excitations in K_2RuCl_6, Phys. Rev. Lett. **127**, 227201 (2021).
[51] H. Gretarsson, H. Fujihara, F. Sato, H. Gotou, Y. Imai, K. Ohgushi, B. Keimer, and H. Suzuki, $J = 1/2$ pseudospins and d-p hybridization in the Kitaev spin liquid candidates RuX_3 (X = Cl, Br, I), Phys. Rev. B **109**, L180413 (2024).
[52] A. H. Abdeldaim, H. Gretarsson, S. J. Day, M. D. Le, G. B. G. Stenning, P. Manuel, R. S. Perry, A. A. Tsirlin, G. J. Nilsen, and L. Clark, Kitaev interactions through extended superexchange pathways in the $J_{\text{eff}} = 1/2$ Ru^{3+} honeycomb magnet RuP_3SiO_{11}, Nat. Commun. **15**, 9778 (2024).
[53] J. Bertinshaw, M. Krautloher, H. Suzuki, H. Takahashi, A. Ivanov, H. Yavaş, B. J. Kim, H. Gretarsson, and B. Keimer, Spin and charge excitations in the correlated multiband metal $Ca_3Ru_2O_7$, Phys. Rev. B **103**, 085108 (2021).
[54] H. Suzuki, L. Wang, J. Bertinshaw, H. U. R. Strand, S. Käser, M. Krautloher, Z. Yang, N. Wentzell, O. Parcollet, F. Jerzembeck, N. Kikugawa, A. P. Mackenzie, A. Georges, P. Hansmann, H. Gretarsson, and B. Keimer, Distinct spin and orbital dynamics in Sr_2RuO_4, Nat. Commun. **14**, 7042 (2023).
[55] H. Gretarsson, H. Suzuki, H. Kim, K. Ueda, M. Krautloher, B. J. Kim, H. Yavaş, G. Khaliullin, and B. Keimer, Observation of spin-orbit excitations and Hund's multiplets in Ca_2RuO_4, Phys. Rev. B **100**, 045123 (2019).
[56] J. Kim, D. Casa, M. H. Upton, T. Gog, Y.-J. Kim, J. F. Mitchell, M. van Veenendaal, M. Daghofer, J. van den Brink, G. Khaliullin, and B. J. Kim, Magnetic excitation spectra of Sr_2IrO_4 probed by resonant inelastic x-ray scattering: Establishing links to cuprate superconductors, Phys. Rev. Lett. **108**, 177003 (2012).
[57] Y. Imai, K. Nawa, Y. Shimizu, W. Yamada, H. Fujihara, T. Aoyama, R. Takahashi, D. Okuyama, T. Ohashi, M. Hagihala, S. Torii, D. Morikawa, M. Terauchi, T. Kawamata, M. Kato, H. Gotou, M. Itoh, T. J. Sato, and K. Ohgushi, Zigzag magnetic order in the Kitaev spin-liquid candidate material $RuBr_3$ with a honeycomb lattice, Phys. Rev. B **105**, L041112 (2022).
[58] K. Nawa, Y. Imai, Y. Yamaji, H. Fujihara, W. Yamada, R. Takahashi, T. Hiraoka, M. Hagihala, S. Torii, T. Aoyama, T. Ohashi, Y. Shimizu, H. Gotou, M. Itoh, K. Ohgushi, and T. J. Sato, Strongly electron-correlated semimetal RuI_3 with a layered honeycomb structure, J. Phys. Soc. Jpn. **90**, 123703 (2021).
[59] D. Ni, X. Gui, K. M. Powderly, and R. J. Cava, Honeycomb-structure RuI_3, a new quantum material related to α-$RuCl_3$, Adv. Mater. **34**, 2106831 (2022).
[60] F. Sato, H. Fujihara, H. Gotou, T. Aoyama, Y. Imai, and K. Ohgushi, Insulator-metal transition in $Ru(Br_{1-x}I_x)_3$ with honeycomb structure, Phys. Rev. B **109**, 035154 (2024).
[61] K. Kanoda and R. Kato, Mott physics in organic conductors with triangular lattices, Annu. Rev. Condens. Matter Phys. **2**, 167 (2011).
[62] C. C. Tam, Near itinerancy and slow singlet formation in the triangular lattice $NaRuO_2$ [dataset], Zenodo, 2026, doi:10.5281/zenodo.21147485.